

From kagome strip to kagome lattice: Realizations of frustrated $S = \frac{1}{2}$ antiferromagnets in Ti(III) fluorides

Harald O. Jeschke,¹ Hiroki Nakano,² and Tôru Sakai^{2,3}

¹Research Institute for Interdisciplinary Science, Okayama University, Okayama 700-8530, Japan

²Graduate School of Material Science, University of Hyogo, Kamigori, Hyogo 678-1297, Japan

³National Institutes for Quantum and Radiological Science and Technology (QST), SPring-8, Sayo, Hyogo 679-5148, Japan



(Received 7 March 2019; published 24 April 2019)

We investigate the connection between highly frustrated kagome based Hamiltonians and a recently synthesized family of materials containing Ti^{3+} $S = \frac{1}{2}$ ions. Employing a combination of all electron density functional theory and numerical diagonalization techniques, we establish the Heisenberg Hamiltonians for the distorted kagome antiferromagnets $\text{Rb}_2\text{NaTi}_3\text{F}_{12}$, $\text{Cs}_2\text{NaTi}_3\text{F}_{12}$, and $\text{Cs}_2\text{KTi}_3\text{F}_{12}$. We determine magnetization curves in excellent agreement with experimental observations. Our calculations successfully clarify the relationship between the experimental observations and the magnetization-plateau behavior at $\frac{1}{3}$ height of the saturation and predict characteristic behaviors under fields that are higher than the experimentally measured region. We demonstrate that the studied Ti(III) family of materials interpolates between the kagome strip and kagome lattice.

DOI: [10.1103/PhysRevB.99.140410](https://doi.org/10.1103/PhysRevB.99.140410)

Introduction. Quantum antiferromagnets on the kagome lattice have fascinated experimental and theoretical physicists for a long time; in particular, since the synthesis of high quality samples of herbertsmithite [1], the search for quantum spin liquid candidates in highly frustrated kagome lattice materials has intensified [2,3]. Cu^{2+} based materials such as $\text{ZnCu}_3(\text{OH})_6\text{Cl}_2$ (herbertsmithite) or $\text{BaCu}_3\text{V}_2\text{O}_8(\text{OH})_2$ (vesignieite) [4] or the vanadium oxyfluoride $[\text{NH}_4]_2[\text{C}_7\text{H}_{14}\text{N}][\text{V}_7\text{O}_6\text{F}_{18}]$ [5] have been at the forefront of the discussion. There are also effects of strong magnetic frustration and unconventional behavior in imperfect kagome lattices such as $\text{ZnCu}_3(\text{OH})_6\text{SO}_4$ [6] or breathing kagome lattices. Recently, an interesting new family of $S = \frac{1}{2}$ kagome materials has been realized based on magnetic Ti^{3+} ions; three compounds $\text{Rb}_2\text{NaTi}_3\text{F}_{12}$, $\text{Cs}_2\text{NaTi}_3\text{F}_{12}$, and $\text{Cs}_2\text{KTi}_3\text{F}_{12}$ have been reported [7]. They are new members of a large class of materials; besides several members involving Cu^{2+} such as the possible valence bond solid $\text{Rb}_2\text{Cu}_3\text{SnF}_{12}$ [8], there are $S = 2$ Mn^{3+} based members such as $\text{Cs}_2\text{LiMn}_3\text{F}_{12}$ [9] and the more recent $S = 1$ V^{3+} based $\text{Cs}_2\text{KV}_3\text{F}_{12}$ [10] or $S = \frac{3}{2}$ Cr^{3+} containing $\text{Cs}_2\text{KCr}_3\text{F}_{12}$ [11]. The Ti^{3+} based materials are particularly attractive because spin orbit coupling is expected to be much smaller than in Cu^{2+} ; thus, in the new $S = \frac{1}{2}$ materials, the Dzyaloshinskii-Moriya interaction which complicates the discussion of many Cu^{2+} based frustrated magnets [12] promises to be much less important.

Theoretically, the $S = \frac{1}{2}$ kagome lattice antiferromagnet has been studied intensively, using density-matrix renormalization group (DMRG) [13], numerical diagonalization [14,15], series expansion methods [16], bosonization [17], and many other techniques. One possible strong distortion of the kagome lattice leads to kagome strips [18] which have been discussed as Δ chains [19] or sawtooth lattices [20] for many years. Recently, kagome strips were

studied using the DMRG technique [21]. It is interesting to look for approximate realizations of kagome strips in real materials. Crystal structures in which the symmetry of the kagome lattice is broken by an orthorhombic distortion are possible candidates for the realization of kagome strips; however, which model is actually realized needs to be discussed at the level of electronic structure rather than crystal structure only.

In this Rapid Communication, we address the problem that while the new $S = \frac{1}{2}$ materials $\text{Rb}_2\text{NaTi}_3\text{F}_{12}$, $\text{Cs}_2\text{NaTi}_3\text{F}_{12}$, and $\text{Cs}_2\text{KTi}_3\text{F}_{12}$ have been characterized structurally and magnetically, their Hamiltonian is essentially unknown. We will apply energy mapping techniques to evaluate the Heisenberg Hamiltonian up to third nearest neighbors in the distorted kagome lattice. We find that the three materials interpolate between a nearly pure Δ chain behavior and an only slightly distorted kagome lattice behavior. Using numerical diagonalization of clusters with up to 36 sites, we obtain excellent agreement with the measured magnetization curves.

Methods. We calculate electronic structure and total energies with the full potential local orbital (FPLO) basis set [22] and the generalized gradient approximation (GGA) functional [23]. Strong electronic correlations in Ti $3d$ orbitals are treated with the GGA+ U [24] exchange and correlation functional. Hund's rule coupling for Ti $3d$ was fixed at $J_H = 0.64$ eV [25]. Heisenberg Hamiltonian parameters are extracted by mapping total energies for 15 different spin configurations to six exchange interactions [26–28].

To obtain magnetization processes, we also carry out numerical diagonalizations of finite-size clusters with Heisenberg interactions determined from the density functional theory calculations. Our numerical diagonalizations are performed based on the Lanczos and/or Householder algorithms in the subspace belonging to $\sum_j S_j^z = M_z$, where the z axis is taken as the quantized axis of each $S = \frac{1}{2}$ spin operator S_j at

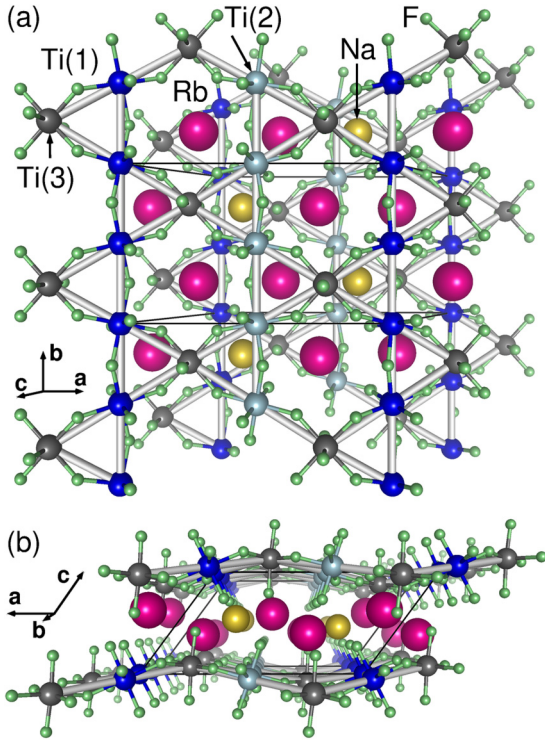


FIG. 1. Crystal structure of $\text{Rb}_2\text{NaTi}_3\text{F}_{12}$ with $P2_1/m$ space group [7]. The kagome lattice formed by the three symmetry inequivalent Ti^{3+} ions Ti(1), Ti(2), and Ti(3) is distorted and buckled.

site j . Our numerical diagonalizations give the lowest energy of the Heisenberg Hamiltonian in the subspace characterized by M_z , which leads to the magnetization curve. (See details in Ref. [29].) Some of the Lanczos diagonalizations were carried out using message passing interface parallelized code that was originally developed in the study of Haldane gaps [30]. The usefulness of our program was confirmed in large-scale parallelized calculations [15,31–41].

Results. Our calculations are based on the structures of isostructural $\text{Rb}_2\text{NaTi}_3\text{F}_{12}$ (shown in Fig. 1), $\text{Cs}_2\text{NaTi}_3\text{F}_{12}$, and $\text{Cs}_2\text{KTi}_3\text{F}_{12}$ as determined by Goto *et al.* [7]. Two Ti^{3+} ion chains running along the crystallographic b axis are different by symmetry. Geometrically, the kagome lattices formed by Ti(1), Ti(2), and Ti(3) sites are only about 1% distorted. However, the decisive factor for the magnetic properties is the electronic distortion, revealed by the result of the energy mapping (Fig. 2). The top of the figure shows the exchange couplings calculated by fitting total energies obtained with the GGA+ U exchange correlation functional as a function of the on-site correlation strength U . We are fitting to the Heisenberg Hamiltonian in the form

$$\mathcal{H} = \sum_{i<j} J_{ij} \mathbf{S}_i \cdot \mathbf{S}_j. \quad (1)$$

Total moments are exact multiples of $1\mu_B$. The energies of the 15 considered spin configurations can be fitted extremely well (see also Ref. [29]), and statistical error bars are smaller than the size of the symbols. Gray vertical lines indicate the interpolated U value at which the set of couplings matches

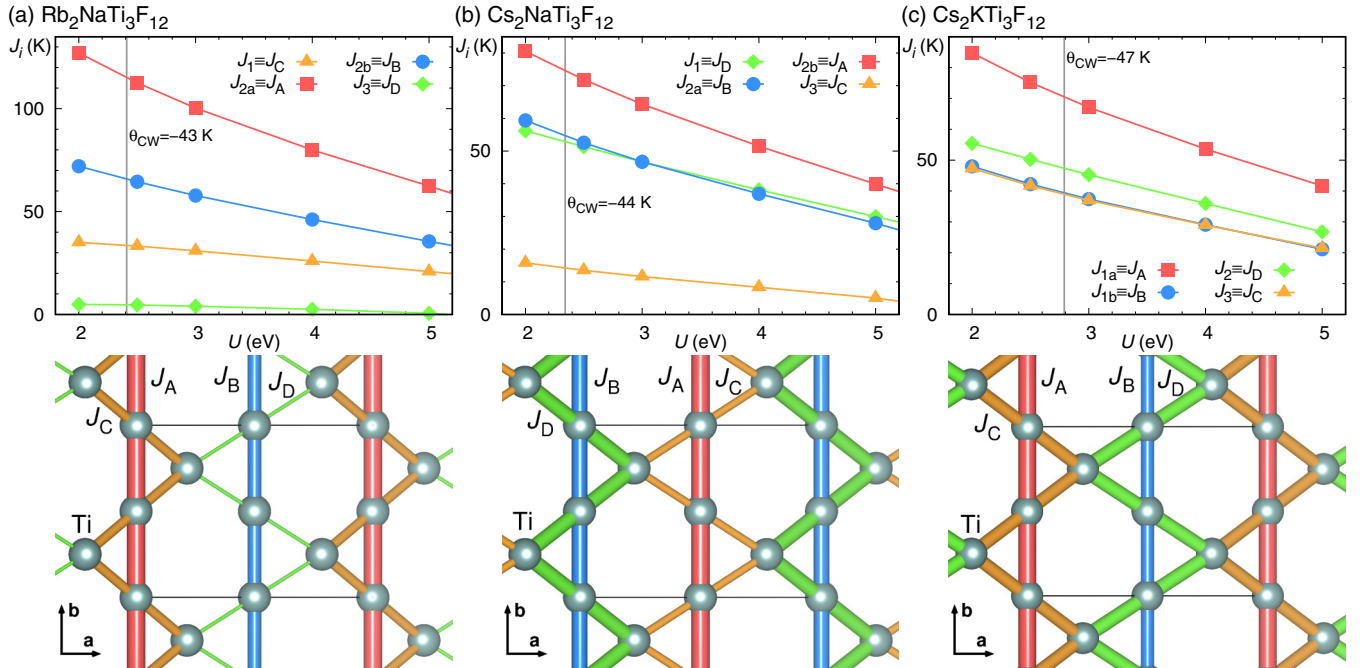


FIG. 2. Heisenberg Hamiltonian parameters for (a) $\text{Rb}_2\text{NaTi}_3\text{F}_{12}$, (b) $\text{Cs}_2\text{NaTi}_3\text{F}_{12}$, and (c) $\text{Cs}_2\text{KTi}_3\text{F}_{12}$ obtained from fits to DFT total energies using a GGA+ U functional for $\text{Ti } 3d$ at $J_H = 0.64$ eV as a function of U . Vertical lines indicate the U value at which the couplings reproduce the experimental Curie-Weiss temperatures Θ_{CW} . J_1 – J_3 label exchange paths geometrically according to increasing Ti-Ti distance $d_{\text{Ti-Ti}}$. J_{2a}/J_{2b} distinguish paths with identical $d_{\text{Ti-Ti}}$ but symmetry inequivalent Ti environments. J_A/J_C label the kagome strip belonging to the largest exchange coupling J_A , and J_B/J_D label the other symmetry inequivalent kagome strip in the unit cell. The structures in the lower panels represent the geometry and the topology; bond cross-sectional areas are proportional to the size of the couplings. A clear evolution from a kagome strip plus 1D chain in $\text{Rb}_2\text{NaTi}_3\text{F}_{12}$ to a slightly distorted 2D kagome model in $\text{Cs}_2\text{KTi}_3\text{F}_{12}$ is observed.

TABLE I. Exchange couplings for $\text{Rb}_2\text{NaTi}_3\text{F}_{12}$, $\text{Cs}_2\text{NaTi}_3\text{F}_{12}$, and $\text{Cs}_2\text{KTi}_3\text{F}_{12}$ determined by energy mapping, using the exchange correlation function $\text{GGA}+U$ with U values that reproduce the experimental Curie-Weiss temperatures $\Theta_{\text{CW}} = -43$ K, $\Theta_{\text{CW}} = -44$ K, and $\Theta_{\text{CW}} = -47$ K, respectively. See Fig. 2 for the assignment of J_A , J_B , J_C , and J_D .

Material	J_A (K)	J_B/J_A	J_C/J_A	J_D/J_A
$\text{Rb}_2\text{NaTi}_3\text{F}_{12}$	115.0	0.572	0.292	0.040
$\text{Cs}_2\text{NaTi}_3\text{F}_{12}$	74.6	0.733	0.190	0.709
$\text{Cs}_2\text{KTi}_3\text{F}_{12}$	70.4	0.558	0.552	0.673

the experimental Curie-Weiss temperature as determined in Ref. [7]. These U values are in the range 2.3–2.8 eV, which is reasonable for Ti. These sets of exchange couplings are listed in Table I. The lower part of Fig. 2 illustrates the obtained Hamiltonians by representing the relative strength of the couplings as the cross-sectional area of the Ti-Ti bonds. The first major result is the observation that the three considered materials realize three quite different Hamiltonians even though they are very similar structurally. The Hamiltonian of $\text{Rb}_2\text{NaTi}_3\text{F}_{12}$ is dominated by an anisotropic kagome strip formed by Ti(1) (J_A) and Ti(3) ($J_C \approx 0.3J_A$) and a one-dimensional (1D) chain of Ti(2) (J_B). In $\text{Cs}_2\text{NaTi}_3\text{F}_{12}$, we have an almost isotropic kagome strip formed by Ti(2) and Ti(3) ions ($J_B \approx J_D$) and, nearly decoupled from that, a one-dimensional chain formed by the Ti(1) ions (J_B). Finally, while in $\text{Cs}_2\text{KTi}_3\text{F}_{12}$ the one-dimensional coupling of Ti(1) ions (J_A) is a bit larger than the other three in-plane couplings, all other couplings in the kagome plane ($J_B \approx J_C \approx J_D$) are also substantial, making $\text{Cs}_2\text{KTi}_3\text{F}_{12}$ a frustrated two-dimensional (2D) antiferromagnet. We also determined two selected interlayer couplings corresponding to fifth- and sixth-nearest-neighbor Ti-Ti distances in the case of $\text{Rb}_2\text{NaTi}_3\text{F}_{12}$, to fifth-nearest-neighbor and ninth-nearest-neighbor in the case of $\text{Cs}_2\text{NaTi}_3\text{F}_{12}$ and to fifth-nearest-neighbor and tenth-nearest-neighbor in the case of $\text{Cs}_2\text{KTi}_3\text{F}_{12}$ [29]. They are so small that they can be neglected in the further discussion.

We now connect the Hamiltonians to the magnetic measurements by carrying out numerical diagonalization calculations for $N = 24$, $N = 30$, and $N = 36$ site clusters. We show $M(H)$ curves for $\text{Rb}_2\text{NaTi}_3\text{F}_{12}$, $\text{Cs}_2\text{NaTi}_3\text{F}_{12}$, and $\text{Cs}_2\text{KTi}_3\text{F}_{12}$ in Figures 3(a)–3(c). The theoretical magnetic field h given in units of J_A is converted to H in tesla using $H = hJ_A/2/0.6717$ T/K. The factor 1/2 is introduced because the DFT determination of the J_i in the Hamiltonian (1) is done without the double counting of bonds. The experimental data points in Fig. 3 are taken from Ref. [7]. Theoretical curves successfully capture the characteristics of the experimental observations in spite of the limitation that our theoretical results have a finite resolution due to the size of the computationally accessible clusters. It is, in particular, clarified that our results at and around the $\frac{1}{3}$ height of the saturation can explain the behavior of the measured $M(H)$ curve for each material, as discussed in detail in the following.

Discussion. A marked feature of the reported experimental result for $\text{Rb}_2\text{NaTi}_3\text{F}_{12}$ shown in Fig. 3(a) is that there appears a considerably large gradient in the $M(H)$ curve from $M = 0$ to approximately $M \sim 0.2$; above $M \sim 0.3$, on

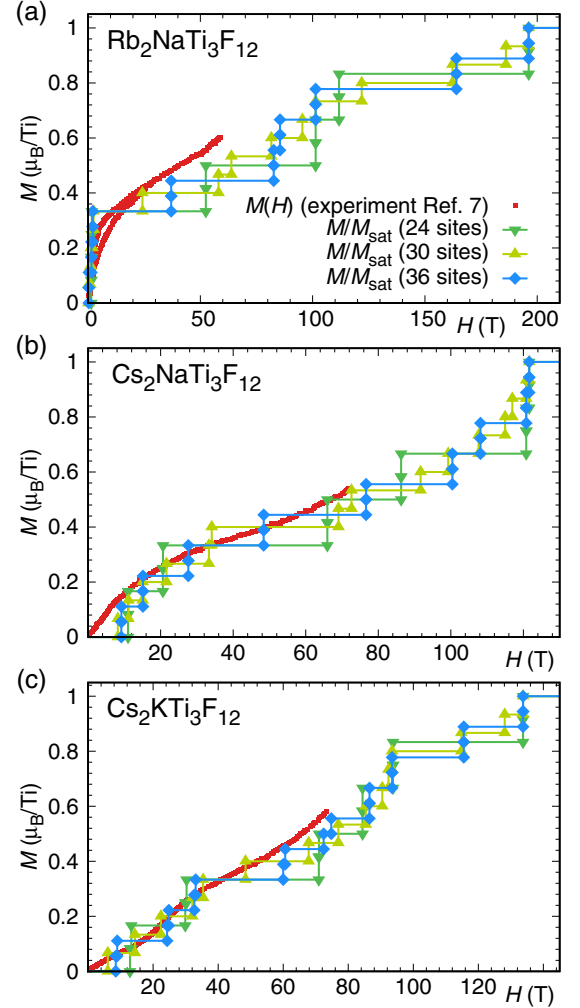


FIG. 3. Comparison between experimental and calculated magnetization curves for all three compounds. The experimental data are from Ref. [7].

the other hand, the $M(H)$ curve shows relatively smaller gradients. Our numerical-diagonalization results reproduce well a very steep gradient below $M = \frac{1}{3}$ and a comparatively small gradient around $M \sim 0.4$ above $M = \frac{1}{3}$. Essentially, a very weak magnetic field is necessary to polarize one-third of the system. Considering our Hamiltonian [see Fig. 2(a)], we have one-third of the spins which are only coupled to the strong J_A chain by the weak J_C bond; as this is a weak and frustrated interaction, a third of the spins are almost free and can easily be polarized, explaining the large $M(H)$ gradients in both experimental and theoretical data. After the initial steep magnetization increase, there is a roughly linear magnetization increase which can be rationalized by the expected initially linear magnetization behavior of the J_B spin chain [42]. Our results suggest that the saturation field is $H \sim 200$ T, which is much larger than the experimentally measured region. Note also that our results predict that a plateau-like behavior appears at $M \sim 0.8$ from approximately 100 T to a field near the suggested saturation. This plateau might arise from a $\frac{1}{2}$ magnetization plateau of the $J_A - J_C$ Δ chain [43], combined with the fully polarized J_B spin chain, i.e., it could be a $\frac{1}{2} + \frac{1}{3} = \frac{5}{6}$ magnetization plateau.

In Fig. 3(b) for $\text{Cs}_2\text{NaTi}_3\text{F}_{12}$, the experimental data show that the gradient at $M = 0$ is larger than gradients around $M \sim 0.4$ but smaller than the steep gradient of $\text{Rb}_2\text{NaTi}_3\text{F}_{12}$ at $M = 0$. Our numerical-diagonalization results, especially around $M = \frac{1}{3}$, capture well these behaviors. The Hamiltonian of $\text{Cs}_2\text{NaTi}_3\text{F}_{12}$ [see Fig. 2(b)] has a spin chain with strong antiferromagnetic J_A and an isotropic Δ chain with $J_B \approx J_D < J_A$. Therefore, the two-thirds of the spins forming the Δ chain are expected to polarize first and reach a $\frac{1}{2}$ magnetization plateau [43] which translates into a $\frac{1}{3}$ magnetization plateau for the full system. Our results suggest that the saturation field is $H \sim 120$ T. Although the height at $M = \frac{2}{3}$ seems as a plateau for $N = 24$, this behavior is considered to be a finite-size phenomenon because the widths for $N = 30$ and 36 become much smaller than that for $N = 24$. At large fields, we find a jump to total magnetization which is expected for both the Δ chain and kagome lattice [44].

Reference [7] reported that $\text{Cs}_2\text{KTi}_3\text{F}_{12}$ shows a concave behavior in the region approximately from 10 to 20 T in its $M(H)$ curve as well as a peak at 23 T in its dM/dH . The peak leads to an abrupt increase of magnetization. The dM/dH for $\text{Cs}_2\text{KTi}_3\text{F}_{12}$ in Ref. [7] reveals an inflection point approximately at 30 T. Since an inflection point in dM/dH corresponds to an edge of a specific plateau at a nonzero temperature, the inflection point at 30 T can be considered to correspond to the edge of the $M = \frac{1}{3}$ plateau on the low-field side. Our theoretical results for the edge are observed around 30–36 T; thus, the experimental and theoretical results agree well with each other. Our theoretical result for $N = 36$ shows a plateaulike behavior with a relatively wider region at $M = \frac{1}{3}$ with a rapid increase of M at the higher-field edge. Our theoretical results are very similar to the experimental observation although it is unclear at present whether or not the behavior of $M = \frac{1}{3}$ corresponds to a spin-gapped behavior. Overall, the model Hamiltonian obtained for $\text{Cs}_2\text{KTi}_3\text{F}_{12}$ [see Fig. 2(c)] corresponds to a kagome lattice with one-third of the spins coupled more strongly than the rest in a one-dimensional chain. This situation is similar but not equal to the one studied in Ref. [45]. Considering the rather complicated magnetization dynamics seen both in experiment and theoretically, the 1D chain (comprising one-third of the spins) coupled in 2D by a weaker kagome lattice might warrant further theoretical study. Our theoretical results also suggest that the saturation field is $H \sim 130$ T and that a plateaulike behavior appears at $M \sim 0.8$ from approximately 90 T to a field near the suggested saturation. Recently, Ref. [46] reported that the measurements of another material $\text{Cs}_2\text{LiTi}_3\text{F}_{12}$, which is a

member of the same family of distorted kagome systems, show a behavior similar to that of $\text{Cs}_2\text{KTi}_3\text{F}_{12}$. In the magnetization curve of $\text{Cs}_2\text{LiTi}_3\text{F}_{12}$, a plateaulike behavior with a height lower than $M = 1/3$ accompanied by the $M = 1/3$ plateau is observed [47]. Investigation of the magnetization curve of the new systems with the methods of the present work will be an interesting future study, strengthening the Ti(III) fluorides as a platform for diverse distorted $S = 1/2$ kagome systems.

Conclusions. We study three kagome-strip materials, $\text{Cs}_2\text{KTi}_3\text{F}_{12}$, $\text{Rb}_2\text{NaTi}_3\text{F}_{12}$, and $\text{Cs}_2\text{NaTi}_3\text{F}_{12}$, by density functional theory and numerical-diagonalization calculations. The $S = \frac{1}{2}$ Hamiltonians revealed by density functional theory based energy mapping indicate that the changes in the alkali metal spacers tune the materials between one- and two-dimensional magnetic behavior. We can show that $\text{Rb}_2\text{NaTi}_3\text{F}_{12}$ approximately realizes an anisotropic Δ chain, and $\text{Cs}_2\text{NaTi}_3\text{F}_{12}$ is close to an isotropic Δ chain. Thus, we have demonstrated that these two materials are very close to realizing important one-dimensional quantum spin systems. Our theoretical results concerning the magnetization curves agree well with experimental results reported in Ref. [7]. By revealing the underlying Hamiltonian, several features of the measured magnetization curves are clarified. Since the present systems reveal a quasi-one-dimensionality in the two-dimensional lattices, the DMRG technique, which was successfully used in Refs. [18,21] on related problems, could provide valuable additional information. By predicting the behavior at higher magnetic fields, we hope to inspire further experimental studies.

Acknowledgments. We wish to thank Professor Kazuyoshi Yoshimura for fruitful discussions. This work was partly supported by JSPS KAKENHI Grants No. 16K05418, No. 16K05419, No. 16H01080 (JPhysics), and No. 18H04330 (JPhysics). Nonhybrid thread-parallel calculations in numerical diagonalizations were based on TITPACK version 2 coded by H. Nishimori. In this research, we used the computational resources of Fujitsu PRIMERGY CX600M1/CX1640M1(Oakforest-PACS) provided by Joint Center for Advanced High Performance Computing through the HPCI System Research project (Project ID No. hp180053). Some of the computations were performed using the facilities of the Department of Simulation Science, National Institute for Fusion Science; Institute for Solid State Physics, The University of Tokyo; and Supercomputing Division, Information Technology Center, The University of Tokyo.

-
- [1] M. P. Shores, E. A. Nytko, B. M. Bartlett, and D. G. Nocera, A structurally perfect $S = 1/2$ kagomé antiferromagnet, *J. Am. Chem. Soc.* **127**, 13462 (2005).
- [2] P. A. Lee, An end to the drought of quantum spin liquids, *Science* **321**, 1306 (2008).
- [3] M. R. Norman, Colloquium: Herbertsmithite and the search for the quantum spin liquid, *Rev. Mod. Phys.* **88**, 041002 (2016).
- [4] Y. Okamoto, H. Yoshida, and Z. Hiroi, Vesignieite $\text{BaCu}_3\text{V}_2\text{O}_8(\text{OH})_2$ as a candidate spin-1/2 kagome antiferromagnet, *J. Phys. Soc. Jpn.* **78**, 033701 (2009).
- [5] F. H. Aidoudi, D. W. Aldous, R. J. Goff, A. M. Z. Slawin, J. P. Attfield, R. E. Morris, and P. Lightfoot, An ionothermally prepared $S = 1/2$ vanadium oxyfluoride kagome lattice, *Nat. Chem.* **3**, 801 (2011).
- [6] Y. Li, B. Pan, S. Li, W. Tong, L. Ling, Z. Yang, J. Wang, Z. Chen, Z. Wu, and Q. Zhang, Gapless quantum spin liquid in the $S = 1/2$ anisotropic kagome antiferromagnet $\text{ZnCu}_3(\text{OH})_6\text{SO}_4$, *New J. Phys.* **16**, 093011 (2014).
- [7] M. Goto, H. Ueda, C. Michioka, A. Matsuo, K. Kindo, and K. Yoshimura, Various disordered ground states and

- $\frac{1}{3}$ magnetization-plateau-like behavior in the $S = \frac{1}{2}\text{Ti}^{3+}$ kagome lattice antiferromagnets $\text{Rb}_2\text{NaTi}_3\text{F}_{12}$, $\text{Cs}_2\text{NaTi}_3\text{F}_{12}$, and $\text{Cs}_2\text{KTi}_3\text{F}_{12}$, *Phys. Rev. B* **94**, 104432 (2016).
- [8] K. Matan, T. Ono, Y. Fukumoto, T. J. Sato, J. Yamaura, M. Yano, K. Morita, and H. Tanaka, Pinwheel valence-bond solid and triplet excitations in the two-dimensional deformed kagome lattice, *Nat. Phys.* **6**, 865 (2010).
- [9] U. Englich, C. Frommen, and W. Massa, Jahn-Teller ordering in Kagomé-type layers of compounds $\text{A}_2\text{A}'\text{Mn}_3^{\text{III}}\text{F}_{12}$ ($\text{A} = \text{Rb}, \text{Cs}$; $\text{A}' = \text{Li}, \text{Na}, \text{K}$), *J. Alloys Compd.* **246**, 155 (1997).
- [10] M. Goto, H. Ueda, C. Michioka, A. Matsuo, K. Kindo, K. Sugawara, S. Kobayashi, N. Katayama, H. Sawa, and K. Yoshimura, Ising-like anisotropy stabilized $\frac{1}{3}$ and $\frac{2}{3}$ magnetization plateaus in the V^{3+} kagome lattice antiferromagnets $\text{Cs}_2\text{KV}_3\text{F}_{12}$, $\text{Cs}_2\text{NaV}_3\text{F}_{12}$, and $\text{Rb}_2\text{NaV}_3\text{F}_{12}$, *Phys. Rev. B* **95**, 134436 (2017).
- [11] M. Goto, H. Ueda, C. Michioka, A. Matsuo, K. Kindo, K. Sugawara, S. Kobayashi, N. Katayama, H. Sawa, and K. Yoshimura, In-plane spin canting and $1/3$ -magnetization-plateau-like behavior in $S = 3/2\text{Cr}^{3+}$ kagome lattice antiferromagnets $\text{Cs}_2\text{KCr}_3\text{F}_{12}$ and $\text{Cs}_2\text{NaCr}_3\text{F}_{12}$, *Phys. Rev. B* **97**, 224421 (2018).
- [12] P. Mendels and F. Bert, Quantum kagome antiferromagnet $\text{ZnCu}_3(\text{OH})_6\text{Cl}_2$, *J. Phys. Soc. Jpn.* **79**, 011001 (2010).
- [13] S. Depenbrock, I. P. McCulloch, and U. Schollwöck, Nature of the Spin-Liquid Ground State of the $S = 1/2$ Heisenberg Model on the Kagome Lattice, *Phys. Rev. Lett.* **109**, 067201 (2012).
- [14] C. Zeng and V. Elser, Numerical studies of antiferromagnetism on a kagomé net, *Phys. Rev. B* **42**, 8436 (1990).
- [15] H. Nakano and T. Sakai, Anomalous behavior of the magnetization process of the $S = 1/2$ kagome-lattice Heisenberg antiferromagnet at one-third height of the saturation, *J. Phys. Soc. Jpn.* **83**, 104710 (2014).
- [16] R. R. P. Singh and D. A. Huse, Three-Sublattice Order in Triangular- and Kagomé-Lattice Spin-Half Antiferromagnets, *Phys. Rev. Lett.* **68**, 1766 (1992).
- [17] A. P. Schnyder, O. A. Starykh, and L. Balents, Spatially anisotropic Heisenberg kagome antiferromagnet, *Phys. Rev. B* **78**, 174420 (2008).
- [18] T. Shimokawa and H. Nakano, Magnetization curve of the kagome-strip-lattice antiferromagnet, *J. Low Temp. Phys.* **170**, 328 (2013).
- [19] T. Nakamura and K. Kubo, Elementary excitations in the Δ chain, *Phys. Rev. B* **53**, 6393 (1996).
- [20] S. A. Blundell and M. D. Núñez-Regueiro, Quantum topological excitations: From the sawtooth lattice to the Heisenberg chain, *Eur. Phys. J. B* **31**, 453 (2003).
- [21] K. Morita, T. Sugimoto, S. Sota, and T. Tohyama, Magnetization plateaus in the spin- $\frac{1}{2}$ antiferromagnetic Heisenberg model on a kagome-strip chain, *Phys. Rev. B* **97**, 014412 (2018).
- [22] K. Koepnik and H. Eschrig, Full-potential nonorthogonal local-orbital minimum-basis band-structure scheme, *Phys. Rev. B* **59**, 1743 (1999); <http://www.FPLO.de>
- [23] J. P. Perdew, K. Burke, and M. Ernzerhof, Generalized Gradient Approximation Made Simple, *Phys. Rev. Lett.* **77**, 3865 (1996).
- [24] A. I. Liechtenstein, V. I. Anisimov, and J. Zaanen, Density-functional theory and strong interactions: Orbital ordering in Mott-Hubbard insulators, *Phys. Rev. B* **52**, R5467(R) (1995).
- [25] T. Mizokawa and A. Fujimori, Electronic structure and orbital ordering in perovskite-type $3d$ transition-metal oxides studied by Hartree-Fock band-structure calculations, *Phys. Rev. B* **54**, 5368 (1996).
- [26] H. O. Jeschke, I. Opahle, H. Kandpal, R. Valentí, H. Das, T. Saha-Dasgupta, O. Janson, H. Rosner, A. Brühl, B. Wolf, M. Lang, J. Richter, S. Hu, X. Wang, R. Peters, T. Pruschke, and A. Honecker, Multistep Approach to Microscopic Models for Frustrated Quantum Magnets: The Case of the Natural Mineral Azurite, *Phys. Rev. Lett.* **106**, 217201 (2011).
- [27] Y. Iqbal, H. O. Jeschke, J. Reuter, R. Valentí, I. I. Mazin, M. Greiter, and R. Thomale, Paramagnetism in the kagome compounds $(\text{Zn}, \text{Mg}, \text{Cd})\text{Cu}_3(\text{OH})_6\text{Cl}_2$, *Phys. Rev. B* **92**, 220404(R) (2015).
- [28] D. Guterding, R. Valentí, and H. O. Jeschke, Reduction of magnetic interlayer coupling in barlowite through isoelectronic substitution, *Phys. Rev. B* **94**, 125136 (2016).
- [29] See Supplemental Material at <http://link.aps.org/supplemental/10.1103/PhysRevB.99.140410> for details of density functional theory and numerical diagonalization calculations and for the full result of the energy mapping.
- [30] H. Nakano and A. Terai, Reexamination of finite-lattice extrapolation of Haldane gaps, *J. Phys. Soc. Jpn.* **78**, 014003 (2009).
- [31] H. Nakano and T. Sakai, Numerical-diagonalization study of spin gap issue of the kagome lattice Heisenberg antiferromagnet, *J. Phys. Soc. Jpn.* **80**, 053704 (2011).
- [32] H. Nakano, S. Todo, and T. Sakai, Long-range order of the three-sublattice structure in the $S = 1/2$ Heisenberg antiferromagnet on a spatially anisotropic triangular lattice, *J. Phys. Soc. Jpn.* **82**, 043715 (2013).
- [33] H. Nakano and T. Sakai, Magnetization process of the spin- S kagome-lattice Heisenberg antiferromagnet, *J. Phys. Soc. Jpn.* **84**, 063705 (2015).
- [34] H. Nakano, Y. Hasegawa, and T. Sakai, Magnetization jump in the magnetization process of the spin- $1/2$ Heisenberg antiferromagnet on a distorted square-kagome lattice, *J. Phys. Soc. Jpn.* **84**, 114703 (2015).
- [35] H. Nakano and T. Sakai, Ferrimagnetism in the spin- $1/2$ Heisenberg antiferromagnet on a distorted triangular lattice, *J. Phys. Soc. Jpn.* **86**, 063702 (2017).
- [36] H. Nakano and T. Sakai, Magnetization process of the spin- $1/2$ triangular-lattice Heisenberg antiferromagnet with next-nearest-neighbor interactions – Plateau or nonplateau, *J. Phys. Soc. Jpn.* **86**, 114705 (2017).
- [37] H. Nakano and T. Sakai, Numerical-diagonalization study of magnetization process of frustrated spin- $1/2$ Heisenberg antiferromagnets in two dimensions: Triangular- and kagome-lattice antiferromagnets, *J. Phys. Soc. Jpn.* **87**, 063706 (2018).
- [38] Y. Hasegawa, H. Nakano, and T. Sakai, Metamagnetic jump in the spin- $1/2$ antiferromagnetic Heisenberg model on the square kagome lattice, *Phys. Rev. B* **98**, 014404 (2018).
- [39] T. Sakai and H. Nakano, Ground state with nonzero spontaneous magnetization of the two-dimensional spin- $1/2$ Heisenberg antiferromagnet with frustration, *AIP Adv.* **8**, 101408 (2018).
- [40] H. Nakano and T. Sakai, Precise estimation of the $S = 2$ Haldane gap by numerical diagonalization, *J. Phys. Soc. Jpn.* **87**, 105002 (2018).

- [41] H. Nakano and T. Sakai, Third boundary of the Shastry-Sutherland model by numerical diagonalization, *J. Phys. Soc. Jpn.* **87**, 123702 (2018).
- [42] R. B. Griffiths, Magnetization curve at zero temperature for the antiferromagnetic Heisenberg linear chain, *Phys. Rev.* **133**, A768 (1964).
- [43] J. Richter, O. Derzhko, and A. Honecker, The sawtooth chain: From Heisenberg spins to Hubbard electrons, *Int. J. Mod. Phys.* **22**, 4418 (2008).
- [44] J. Schulenburg, A. Honecker, J. Schnack, J. Richter, and H.-J. Schmidt, Macroscopic Magnetization Jumps due to Independent Magnons in Frustrated Quantum Spin Lattices, *Phys. Rev. Lett.* **88**, 167207 (2002).
- [45] H. Nakano, T. Shimokawa, and T. Sakai, Collapse of ferrimagnetism in two-dimensional Heisenberg antiferromagnet due to frustration, *J. Phys. Soc. Jpn.* **80**, 033709 (2011).
- [46] R. Shirakami, M. Goto, H. Ueda, A. Matsuo, K. Kindo, C. Michioka, and K. Yoshimura, Systematic variations of structure and magnetism in $S = 1/2$ kagome lattice antiferromagnets $A_2B\text{Ti}_3\text{F}_{12}$ (A, B : monovalent cations), JPS autumn meeting 2018, 9aPS-70 (unpublished).
- [47] K. Yoshimura (private communication).